# Charge Transfer Exciton and Spin Flipping at Organic-Transition Metal Dichalcogenide Interfaces

Tika R. Kafle, Bhupal Kattel, Samuel D. Lane, Ti Wang, Hui Zhao, and Wai-Lun Chan\*

Department of Physics and Astronomy, University of Kansas, Lawrence, KS 66045, US

#### **Abstract**

Two-dimensional transition-metal dichalcogenides (TMD) can be combined with other materials such as organic small molecules to form hybrid van der Waals heterostructures. Because of different properties possessed by these two materials, the hybrid interface can exhibit properties that cannot be found in either of the materials. In this work, the zinc phthalocyanine (ZnPc) – molybdenum disulfide (MoS<sub>2</sub>) interface is used as a model system to study the charge transfer at these interfaces. It is found that the optically-excited singlet exciton in ZnPc transfers its electron to MoS<sub>2</sub> in 80 fs after photoexcitation to form a charge transfer exciton. However, back electron transfer occurs on the timescale of  $\sim 1-100$  ps, which results in the formation of a triplet exciton in the ZnPc layer. This relative fast singlet-triplet transition is feasible because of the large singlet-triplet splitting in organic materials and the strong spin-orbit coupling in TMD crystals. The back electron transfer would reduce the yield of free carrier generation at the heterojunction if it is not avoided. On the other hand, the spin-selective back electron transfer could be used to manipulate electron spin in hybrid electronic devices.

Keywords: charge transfer, transition-metal dichalcogenide, organic molecules, van der Waals heterostructures, spin, photoemission spectroscopy

Two-dimensional (2D) layered materials have attracted much attention recently because of the feasibility in stacking layers with different properties together via weak van der Waals forces, which enables the "materials by design" concept to be realized in the nanoscale. Because of their semiconducting property, 2D transition metal dichalcogenide (TMD) layered crystals have been used to create different optoelectronic devices. 1-4 However, fabricating uniform 2D heterostructures with a large area is still a major challenge to overcome. A viable alternative is to combine 2D crystals with other materials to form hybrid heterostructures.<sup>5-6</sup> One example is the organic-TMD heterostructure in which the constituents of both materials are bonded together by the van der Waals interaction. Some previous works take advantage of organic-2D interfaces to create well-ordered organic films with improved transport properties.<sup>7-8</sup> One can further envision that properties of organic materials can be incorporated to create functions that cannot be found in all-2D heterostructures. For example, a singlet exciton (with a total spin of 0) can have a significantly higher energy than a triplet exciton (with a total spin of 1) in many organic semiconductors because of the strong exchange interaction. This results in interesting properties such as singlet fission that can improve the solar cell performance beyond the Shockey-Queisser limit. 2D materials would be used to extract the multiple carriers generated by the singlet fission. 10 Moreover, because of its weak spin-orbit coupling, organic materials usually have a long spin relaxation time. 11-13 This means that an excited electron in organic materials would maintain the same spin state for a long period of time. The long spin relaxation time of organic materials would combine with the spin and pseudospin properties of TMD crystals 14-16 to produce next generation spintronic devices. While there have been a number of works devoted to understand the charge transfer (CT) dynamics at 2D-heterostructures, <sup>17-19</sup> relative few studies have been done to understand these dynamical processes at organic-TMD interfaces.

Recent photo-luminescence quenching studies<sup>20-21</sup> and device measurements<sup>22-25</sup> have demonstrated that effective CT can occur at organic-TMD interfaces. However, there is limited time-resolved measurements on the CT processes at these interfaces. 26-27 A detailed understanding of interfacial CT processes is critical for improving the efficiency of opto-electronic devices built with organic-TMD heterostructures. In this work, steady-state and time-resolved photoemission spectroscopy are used to study the energetics and the CT properties at organic-TMD interfaces. For the zinc phthalocyanine (ZnPc) -MoS<sub>2</sub> interface that is being investigated, it is found that optically-excited electrons in ZnPc transfer to MoS2 within 80 fs after photoexcitation to produce interfacial CT excitons (or sometimes known as indirect or interlayer excitons). Moreover, the transferred electrons undergo back electron transfer (BET) from MoS<sub>2</sub> to ZnPc to form triplet (T<sub>1</sub>) excitons in ZnPc. Significant T<sub>1</sub> population can be found within a few ps after photoexcitation, which is much shorter than the intersystem crossing time  $(100 \text{ ps} - 1 \text{ ns})^{28}$  of ZnPc. The observed ultrafast T<sub>1</sub> formation at the interface is resulted from a combination of the strong spin-orbit coupling in MoS<sub>2</sub> and the large singlet-triplet splitting in ZnPc. The strong spin-orbit coupling in MoS<sub>2</sub> allows the transferred electron to flip to the opposite spin state in a relative short period of time. The large singlet-triplet splitting in ZnPc (the  $T_1$  state is located at  $\sim 0.6$  eV below the optically-excited singlet  $(S_1)$  state) provides the driving force for the BET and  $T_1$  formation once the spin flipping occurs in the MoS<sub>2</sub> layer.

Controlling the spin state of excitons is important for the design of effective organic light emitting diodes<sup>29</sup> and photovoltaics.<sup>30</sup> For optoelectronic and photovoltaic devices, the formation of  $T_1$  excitons resulting from BET can be a loss channel that reduces the number of free carriers. Therefore, this process needs to be avoided. On the other hand, the formation of spin-triplet excitons can sometime be desirable because it can prohibit radiative recombination and can

significantly enhance the exciton lifetime.<sup>30</sup> Therefore, understanding the CT and spin flipping processes at organic-TMD interfaces is important for various opto-electronic applications. Moreover, the spin relaxation time in organic crystals can be on the order of ns -  $\mu$ s.<sup>12</sup> At organic-TMD interfaces, long-lived, spin-polarized carriers in the organic crystal would selectively remove electrons with a certain spin orientation from the TMD layer *via* the formation of T<sub>1</sub> in the organic layer. Hence, the organic-TMD interface would provide a platform to study spin-valley physics in TMD crystals by taking advantage of the long spin relaxation time found in organic crystals.

## **RESULTS AND DISCUSSION**

In this study, the interface formed by ZnPc and bulk, single crystal MoS<sub>2</sub> is chosen as the model system to study the electron dynamics at the organic-TMD interface. We note that bulk MoS<sub>2</sub> has certain properties that are different from the monolayer MoS<sub>2</sub>. For example, bulk MoS<sub>2</sub> has an indirect band gap and a much smaller exciton binding energy. This is in contrast to the direct band gap<sup>31</sup> and the strong exciton binding<sup>32-33</sup> found in the monolayer MoS<sub>2</sub>. Despite these differences, we expect that similar CT processes can occur at organic-monolayer-TMD interfaces if the interface has the required band alignment as discussed below. In particular, the CT processes studied by this work involve states with energies close to the conduction band minimum (CBM) of MoS<sub>2</sub> (*i.e.* states near K points and halfway between  $\Gamma$  and K points). It is known that the electronic wavefunction of these states is mainly oriented in the in-plane direction.<sup>34</sup> In contrast to states near the  $\Gamma$ -point, the energy and wavefunction of these states are less affected by the MoS<sub>2</sub> interlayer coupling.<sup>34</sup> Indeed, the BET process would be favored by factors such as the spatial confinement of the electronic wavefunction and the stronger exciton binding that are found in the

monolayer-TMD. On the other hand, the spin flipping process that is necessary for the  $S_1$ - $T_1$  transition would be slower in the monolayer-TMD because of its longer spin relaxation time.<sup>15</sup>

ZnPc molecules are deposited on a single crystal MoS<sub>2</sub> substrate in an ultra-high vacuum (UHV) chamber to form a type-II heterostructure. Sample preparation procedures can be found in the method section. Figure 1a shows the diffraction pattern of the bulk MoS<sub>2</sub> single crystal measured by low energy electron diffraction (LEED) prior to ZnPc deposition. Because LEED is a surface sensitive technique, the sharp diffraction pattern indicates that the as-prepared MoS<sub>2</sub> surface is clean and has no significant molecular contaminate. The LEED pattern for 1 nm of ZnPc deposited on MoS<sub>2</sub> is shown in Figure 1b. The in-plane spacing between ZnPc molecules can be determined from the diameter of the smallest diffraction ring in the LEED pattern, which is found to be 13.2Å. This lattice spacing agrees with previous STM studies of metal-phthalocyanine on MoS<sub>2</sub>. The result shows that ZnPc molecules have a face-on orientation with respect to the MoS<sub>2</sub> surface. The ionization potential (IP) of thicker ZnPc thin films determined from the ultraviolet photoemission spectroscopy (UPS) is 5.14 eV (supporting information), which is consistent with the reported IP of lying-down metal-phthalocyanine molecules.

After establishing the orientation of ZnPc molecules, UPS is used to determine the band alignment at the ZnPc-MoS<sub>2</sub> interface. Figure 1c shows a series of UPS spectra for samples with different ZnPc thicknesses. The photoelectrons are collected at an emission angle along the surface normal direction. For the bulk MoS<sub>2</sub> crystal, the spectrum represents the density of state at the  $\Gamma$  point. The binding energy in the UPS spectra is referenced with respect to the Fermi level ( $E_F$ ). In the MoS<sub>2</sub> spectrum (red line), the Mo-4d band (solid triangle) and the valence band maximum (VBM) can be identified.<sup>38</sup> After the deposition of 0.5 nm of ZnPc, the highest occupied molecular orbital (HOMO) of ZnPc, which has a smaller binding energy than the MoS<sub>2</sub>-VBM, is observed in

the spectrum (labelled with the blue vertical line). Because the spectral features from both MoS<sub>2</sub> and ZnPc are visible in the 1 nm ZnPc spectrum, this spectrum is used primarily to determine the interfacial band alignment that is shown in Figure 1d. In the presence of the ZnPc molecules, the Mo-4d band (labelled by pink triangles) shifts towards  $E_F$  by  $\sim 0.24$  eV. This shift would be caused by p-doping in MoS<sub>2</sub> after the ZnPc deposition. The MoS<sub>2</sub>-VBM should incur the same energy shift, although the VBM cannot be identified easily in the 0.5 nm or the 1 nm spectra. The energy positions of the MoS<sub>2</sub>-VBM (after accounting for the energy shift caused by the ZnPc deposition) and the ZnPc-HOMO as determined from the spectrum are shown in Figure 1d. For thicker ZnPc films, the HOMO shifts to higher binding energies (Figure 1c). The ZnPc-HOMO position as a function of the ZnPc thickness is shown in the supporting information.

Bulk  $MoS_2$  has an indirect band gap of 1.3 eV.<sup>39</sup> This value is used to determine the location of the conduction band minimum (CBM) of  $MoS_2$  shown in Figure 1d. As it will be shown, the position of the optically-excited  $S_1$  state of ZnPc can be determined from the time-resolved two photon photoemission (TR-TPPE) spectrum. For the 1 nm-thick sample, the  $S_1$  state is at ~1.7 eV above the ZnPc's HOMO. This value agrees well with the energy of the  $S_1$  peak in the optical absorption spectrum.<sup>40</sup> The energy position of the ZnPc  $S_1$  state is indicated in Figure 1d. An energy scale that is referenced with respect to the ZnPc HOMO is shown on the right. This scale will be used in the TR-TPPE spectra. The  $MoS_2$ -ZnPc interface forms a typically type-II heterostructure. Hence, if the  $S_1$  state of ZnPc is optically excited, the excited electron is expected to transfer from ZnPc to the conduction band of the  $MoS_2$  crystal.

To verify the occurrence of CT from ZnPc to MoS<sub>2</sub>, we perform photoluminescence (PL) measurements for 2 nm ZnPc films grown on SiO<sub>2</sub> (300 nm)/Si and MoS<sub>2</sub> substrates. In the PL experiment, an excitation wavelength of 633 nm (~1.96 eV) is used. The PL spectra for the two

samples are shown in Figure 1e. In these PL spectra, the background signal taken from the bare substrate is subtracted. For the ZnPc on  $SiO_2/Si$  sample, a PL peak at  $\sim 680$  nm can be observed, which corresponds to the energy of the  $S_1$  exciton. Ultrafast CT at the ZnPc-Mo $S_2$  interface can quench the  $S_1$  population in ZnPc, resulting in the disappearance of the PL peak. As shown in Figure 1e, the PL intensity at  $\sim 680$  nm is below the detection limit for the 2 nm ZnPc film grown on Mo $S_2$ . Hence, the PL intensity is quenched at least by a factor of 10 in the ZnPc-Mo $S_2$  sample.

TR-TPPE spectroscopy is used to measure the interfacial CT dynamics. Similar to other femtosecond (fs) time-resolved pump-probe techniques, a pump pulse is used to excite valance electrons and a probe pulse is used to determine the population and the nature of excited states. A pump pulse, with a photon energy centered at 1.77 eV chosen to match the S<sub>1</sub> energy of ZnPc, is used to excite the sample. In the TR-TPPE method, a time-delayed UV probe pulse is used to ionize the optically-excited electron and the kinetic energy of the ionized electron is measured by an electron analyzer. The energy of the excited state can be determined from the kinetic energy of the ionized electron and the probe photon energy using conservation of energy. Details of typical TR-TPPE setups can be found in Ref. [41]. In our TPPE spectra, because the signal is mainly originated from the ZnPc layer, the energies for excited states will be referenced with respect to the ZnPc-HOMO (i.e. the energy scale shown on the right side of Figure 1d).

Figure 2a-b show the TR-TPPE spectrum for 0.5 nm of ZnPc deposited on MoS<sub>2</sub> on two different timescales. The pseudocolor represents the intensity of the TPPE signal. In Figure 2a, a peak at E-E<sub>HOMO</sub>  $\sim 1.8$  eV can be found at t = 0. This energy agrees with the S<sub>1</sub> energy measured by optical absorption spectroscopy. <sup>40</sup> Hence, it is assigned to the S<sub>1</sub> state in ZnPc. This state has a very short lifetime (< 100 fs). As we will explain, the disappearance of the S<sub>1</sub> signal can be attributed to the CT from ZnPc to MoS<sub>2</sub>. This CT time is comparable to those found in organic-

graphene interfaces. 42-43 At larger delay times (Figure 2(b)), a peak at ~ 1.3 eV emerges in the spectrum. As it will be shown, its intensity continues to rise on the 10 - 100 ps timescale. Similar behaviors can be observed when the thickness of ZnPc is increased to 1 nm (Figure 2c). Note that the  $S_1$  peak (at ~1.7 eV) and the low energy peak (at ~1.2 eV) shift to slightly lower energies as compared to the 0.5 nm sample. This can be explained by the dielectric screening from the substrate, which can shift energy levels of molecules neighboring the MoS<sub>2</sub>.<sup>44</sup> The intensity of the low energy peak is more pronounced in the 1 nm sample as compared to that in the 0.5 nm sample. Because the photoemission probe is surface sensitive, the strong intensity of this peak indicates that it is likely originated from the overlaying ZnPc layer. ZnPc has a T<sub>1</sub> state at 1.1 eV above HOMO, 45 which matches the position of this low energy peak. Therefore, this peak is assigned to the ZnPc-T<sub>1</sub> state. The T<sub>1</sub> state can be populated by BET from MoS<sub>2</sub> to ZnPc after the orientation of the spin is flipped. Spin-flipping can occur more rapidly in MoS<sub>2</sub> than in ZnPc because of the strong spin-orbit coupling in MoS<sub>2</sub>. In ZnPc, the timescale for S<sub>1</sub>-T<sub>1</sub> transition is on the order of  $100 \text{ ps} - 1 \text{ns.}^{28}$  Indeed, as we will discuss, we do not observe the formation of  $T_1$  in our ZnPc films deposited on  $SiO_2/Si$ . In contrast, the reported spin relaxation time in  $MoS_2$  is in the range of  $\sim 1-10$  ps,  $^{46-47}$  except for very low temperatures (< 50 K) in which a spin relaxation time on the order of 1 ns has been reported. 48

We have performed TR-TPPE experiments on the bare MoS<sub>2</sub> crystal and we observe a much weaker TPPE signal that is below our detection limit (supporting information). Two factors can contribute to the weak TPPE signal from the MoS<sub>2</sub> crystal. The first factor relates to the amount of electrons that can be excited optically in MoS<sub>2</sub> by the pump pulse. The second one relates to the sensitivity of our TPPE probe to electronic states near the CBM of MoS<sub>2</sub>. First, although the bulk

MoS<sub>2</sub> has an indirect bandgap of 1.3 eV, the absorption coefficient is much smaller due to the indirect nature of the bandgap. The minimum energy needed for direct optical transition in MoS<sub>2</sub> is ~ 1.9 eV, <sup>31, 39, 49</sup> which is larger than our pump photon energy (1.77 eV). Therefore, the concentration of photoexcited electrons induced by the pump pulse in MoS2 is expected to be much lower than that in ZnPc. Second, electronic states near the CBM of MoS<sub>2</sub> have large momentums in k-space. To fulfill momentum conservation in the photoionization process<sup>50</sup> (the probe process), a probe photon energy of  $\sim 10-20$  eV is required for the photoionization if no other excitation, such as a phonon, is involved. 51-52 Our probe photons only have an energy of 4.68 eV, which is not enough energy to ionizes these electrons via a direct optical process. Hence, our probe is not sensitive to excited electrons in MoS<sub>2</sub>. The first factor suggests that the pump excites ZnPc primarily and the observed signal should be dominated by excited electrons originated from the ZnPc layer. For the ZnPc-MoS<sub>2</sub> samples, the second factor, i.e. the low sensitivity of the TPPE probe to excited electrons in MoS2, causes a rapid decay in the photoemission intensity after the CT process. This is because the sensitivity of the probe to an excited electron is much reduced when the electron transfers from ZnPc to MoS<sub>2</sub>.

For an even thicker ZnPc layer, because photoemission is a surface sensitive technique, only excitons near the ZnPc surface are probed. Figure 2d shows the TR-TPPE spectrum for a 10 nm-ZnPc on MoS<sub>2</sub> sample. The lifetime of the S<sub>1</sub> state (at  $\sim$  1.7 eV) is orders of magnitude longer than that observed in the 1 nm and 0.5 nm samples. In the 10 nm-ZnPc sample, excitons in the surface region need to diffuse to the ZnPc-MoS<sub>2</sub> interface before CT can occur. The time needed for the exciton to diffuse a distance of  $\sim$  10 nm is rather long (> 100 ps).<sup>53</sup> Therefore, the TR-TPPE spectrum for the 10 nm sample essentially represents the exciton dynamics of a standalone ZnPc thin film. The much longer S<sub>1</sub> lifetime observed in the 10 nm sample further supports that

than the intrinsic property of the ZnPc film. Moreover, unlike samples with a thin ZnPc layer, no clear  $T_1$  state is observed in the 10 nm spectrum. This is consistent to previous works in which the intersystem crossing in ZnPc is found to occur on the 100 ps – 1 ns timescale.<sup>28</sup> Therefore, the CT from ZnPc to MoS<sub>2</sub>, the spin flipping in MoS<sub>2</sub> and the BET to ZnPc together provide an ultrafast kinetic pathway for the  $S_1$ - $T_1$  transition at the ZnPc-MoS<sub>2</sub> interface. This is in contrast to the  $S_1$ - $T_1$  transition in a standalone ZnPc film, which occurs on a much longer timescale.

To further understand the details of the CT and S<sub>1</sub>-T<sub>1</sub> transition dynamics, the TPPE spectra for the 0.5 nm sample at some representative delay times are plotted in Figure 3a. At t = 0ps, it is found that the S<sub>1</sub> peak of ZnPc is populated upon optical excitation. The S<sub>1</sub> peak has a broad low energy tail, which is similar to the S<sub>1</sub> spectrum observed in our previous work.<sup>54</sup> The S<sub>1</sub> population decays with a sub-100 fs time constant, as evidenced by the disappearance of the S<sub>1</sub> peak in the 0.1 ps spectrum. We attribute the decay of the  $S_1$  state to the CT to MoS<sub>2</sub>. At  $t \sim 0.3$  – 1 ps, a peak at  $E - E_{HOMO} \sim 1.5 - 1.6$  eV (pink spectra) emerges which eventually transitions into a more intense  $T_1$  peak at ~ 1.3 eV on the ps timescale (blue spectra). As we will show, the intensity of the  $T_1$  peak continues to grow on the 10 - 100 ps timescale, but at a slower rate. As mentioned earlier, the T<sub>1</sub> state can be populated by BET from MoS<sub>2</sub> to ZnPc after the spin of the electron is flipped in  $MoS_2$ . The peak near 1.5 - 1.6 eV is then assigned to the CT state with the excited electron residing in the MoS<sub>2</sub> layer. The energy of the assigned CT state is  $\sim 0.3$  eV higher than the CBM of MoS<sub>2</sub> (Figure 1d). It is known that hot carrier relaxation is rather slow in bulk-MoS<sub>2</sub> (on the order of  $\sim 10$  ps). <sup>55-56</sup> At  $t \sim 0.3 - 1$  ps (when the CT peak is apparent), it is likely that the transferred electron in MoS<sub>2</sub> has not fully relaxed to the CBM after the initial CT process. Moreover, a recent theoretical calculation<sup>24</sup> shows that the binding energy of CT excitons at organic-TMD interfaces is rather weak (< 40 meV). Exciton binding is not likely to lower the electron energy significantly. The low intensity of the CT feature is consistent with our earlier argument that the photoionization of electrons from the MoS<sub>2</sub> layer has a weak ionization cross section. For the spectra obtained from the 1 nm-ZnPc sample, we cannot identify this CT peak (supporting information) and the low energy spectral region is dominated by a wider T<sub>1</sub> peak. The intensity of the CT peak becomes weaker for a thicker overlaying ZnPc layer, which is consistent with the surface sensitive nature of the photoemission probe.

Figure 3b shows the temporal evolution of the normalized peak intensity of the S<sub>1</sub> peak for various ZnPc thicknesses. For thin (0.5 nm, 1 nm) ZnPc samples, the initial rapid decay is attributed to CT to MoS<sub>2</sub>. An exponential fit yields a decay time of 80 fs (dashed line). For thicker samples (4 nm and 10 nm), the excitons in the surface region need to diffuse to the interface before CT can occur. As mentioned earlier, incoherent exciton diffusion to the interface occurs on a much longer timescale. Therefore, the rapid decay originated from the CT is not observed for these thicknesses. Indeed, for these thicker ZnPc samples, the dynamic closely resembles to those found in 10 nm of ZnPc deposited on a SiO<sub>2</sub>/Si substrate (black curve). The spectrum for 1 nm ZnPc on SiO<sub>2</sub>/Si, which also shows a long S<sub>1</sub> lifetime, is included in the supporting information. No CT is expected at the ZnPc/SiO<sub>2</sub> interface. Therefore, the result from the 10 nm-ZnPc/MoS<sub>2</sub> sample essentially represents the dynamics in a standalone ZnPc film.

Figure 3c shows the temporal evolution of the intensity around the  $T_1$  peak for different ZnPc thicknesses. The intensity is normalized by the intensity at  $t \sim 0$  ps. Note that the intensity near t = 0 is not zero because the  $S_1$  peak has a broad low energy tail that overlaps with the  $T_1$  peak (Figure 3a). For all samples, the  $T_1$  intensity continues to grow up to the longest time (300 ps) that is accessible by our setup. The rise times determined from a bi-exponential fit (dashed

line) to the 1 nm data are 2.7 ps and 81 ps (see supporting information for the fitting parameters). The creation of the T<sub>1</sub> state involves two processes: the spin flipping in MoS<sub>2</sub> and the subsequent BET to ZnPc. The rise time of the T<sub>1</sub> intensity can be controlled by either of these processes. For example, the bi-exponential rise would be originated from the formation of a manifold of CT states with different delocalization sizes<sup>24, 54</sup> and each of these CT states has different BET kinetics. Another possible cause for the multiple rise times would be the dependence of the spin relaxation time on the spin direction. At the MoS<sub>2</sub> layer adjacent to ZnPc, the breaking of the inversion symmetry can lead to momentum-dependent spin splitting<sup>57</sup> similar to that found in monolayer MoS<sub>2</sub>. For monolayer MoS<sub>2</sub>, the out-of-plane spin (relative to the MoS<sub>2</sub> plane) and the in-plane spin can have different relaxation mechanisms.<sup>46</sup> Theoretical model shows that the out-of-plane spin relaxation time is an order of magnitude longer than the in-plane spin relaxation time. The calculated spin relaxation times for in-plane (a few ps) and out-of-plane (10s of ps)<sup>46</sup> spins are consistent to our measured T<sub>1</sub> rise times.

A strong  $T_1$  intensity is observed in Figure 3c for the 0.5 nm and 1 nm sample. The intensity becomes much weaker for the 4 nm sample. In the 4 nm spectrum, a major portion of the intensity is contributed by the  $S_1$  state because of the spectral overlapping with the longer-lived  $S_1$  state. Again, because photoemission is a surface sensitive probe, any triplet formed at the interface must diffuse to the surface before it can be detected. Triplet diffusion is a rather slow process, which justifies the weak  $T_1$  intensity observed in the 4 nm sample. For the 10 nm sample, we do not observe a clear  $T_1$  intensity emerges from the spectrum. The diminishing of the  $T_1$  intensity in thicker films further confirms that the triplets are generated at the interface.

We have also investigated the CT dynamics at the ZnPc-bulk WSe<sub>2</sub> interface. Same experimental methods as those used for MoS<sub>2</sub> are used to study the WSe<sub>2</sub> sample. Our UPS

spectra (included in the supporting information) indicate that the ZnPc-bulk WSe<sub>2</sub> interface has a type-I band alignment. Figure 4a shows the band alignment at the interface determined from the UPS spectra. The indirect gap of bulk-WSe2 is taken to be 1.2 eV.58 Figure 4b shows the TR-TPPE spectrum for the 1 nm ZnPc on WSe<sub>2</sub> sample. A short-lived S<sub>1</sub> state at  $\sim 1.7$  eV can be observed. Similar to the ZnPc-MoS<sub>2</sub> interface, the decay of the S<sub>1</sub> signal can be assigned to the CT from ZnPc to WSe<sub>2</sub>. The intensity of the S<sub>1</sub> state as a function of time is shown in Figure 4c. An exponential fit (dashed line) yields a lifetime of 230 fs. The decay time is slower than that observed in the ZnPc-MoS<sub>2</sub> sample. The ZnPc-S<sub>1</sub> state and the WSe<sub>2</sub>-CBM has a smaller energy offset compared to the offset at the ZnPc-MoS<sub>2</sub> interface. Because only states with energies between the ZnPc-S<sub>1</sub> and the WSe<sub>2</sub>-CBM can accept electrons from ZnPc, fewer states in WSe<sub>2</sub> are available to accept electrons. This can result in a reduced CT rate. Because of the type-I band alignment, the  $S_1$  decay can also be originated from energy transfer. Notably, no pronounced  $T_1$ state is observed in the ZnPc-WSe<sub>2</sub> spectrum. The type-I band alignment allows both electron transfer and hole transfer from ZnPc to WSe<sub>2</sub> to occur. Both transfers should happen on similar time scales (hundreds of fs). Without a hole in ZnPc, BET from WSe<sub>2</sub> to ZnPc is not energetically feasible because the back-transferred electron cannot recombine with a hole in ZnPc to form a low energy  $T_1$  exciton.

In Figure 4b, a peak near  $\sim 1.4 - 1.5$  eV can also be observed. This peak has a longer lifetime, which is attributed to the optically-excited electrons in WSe<sub>2</sub>. Unlike MoS<sub>2</sub>, the lowest energy, intense optical absorption peak in WSe<sub>2</sub> is at a photon energy of  $\sim 1.6$  eV,<sup>59</sup> which is smaller than the 1.77 eV pump photon energy. The relative high concentration of optically-excited electrons in WSe<sub>2</sub> allows them to be visible in the TPPE spectrum. The TR-TPPE spectrum for the

bare WSe<sub>2</sub> substrate is included in the supporting information. A similar long-lived feature near the WSe<sub>2</sub> CBM is observed.

To further understand the BET and the triplet formation process, the temporal evolution of the  $T_1$  intensity is measured for different pump laser fluences. In the BET process, if the original electron-hole pair in a  $S_1$  exciton recombines to form the  $T_1$  exciton (germinate recombination), the process is first-order and the kinetics is independent of the pump fluence. On the other hand, if an electron excited independently in  $MoS_2$  transports to the interface and combines with a residue hole in the ZnPc (non-germinate recombination), the process is second-order and the kinetics should depend on the pump fluence. Pump laser fluences of 4.4, 14 and 42  $\mu$ J cm<sup>-2</sup> are used to study the triplet formation dynamics in the 1 nm-ZnPc sample. The intensity is normalized so that the kinetics can be compared. The kinetic traces for different fluences are shown in Figure 5. We found that the kinetics is almost identical for different pump fluences. The inset in Figure 5 plots the actual TPPE intensity at t = 200 ps as a function of the pump laser fluence, which shows a linear dependence. This behavior indicates that the triplet formation is a first-order process, which is presumably due to germinate recombination.

Based on these findings, we propose that after the initial CT from ZnPc to MoS<sub>2</sub>, the electron-hole pair does not dissociate fully into free carriers, but instead, they form a CT exciton at the interface. The spin of the transferred electron can be flipped in MoS<sub>2</sub>. After the spin-flipping, the BET becomes energetic feasible *via* the formation of a lower energy triplet in ZnPc. Note that if the CT exciton dissociates before the BET, the hole in ZnPc and the electron in MoS<sub>2</sub> that form the T<sub>1</sub> exciton will be independent from each other. In this case, the BET will be a second-order non-germinate process. This is inconsistent to the measured dynamics, which is independent of the fluence. Moreover, the pump pulse can also generate free electrons and holes in MoS<sub>2</sub>. These

electrons in MoS<sub>2</sub> would recombine with the residue holes in ZnPc to produce triplets. However, this recombination channel is non-germinate and it does not agree with the observed fluence dependence. As mentioned earlier, bulk MoS<sub>2</sub> has an indirect bandgap. Although our pump photon energy is larger than the indirect bandgap, it is smaller than the lowest energy required for direct optical transition.<sup>49</sup> Hence, the concentration of optical-excited carriers in MoS<sub>2</sub> should be relative low compared to the exciton concentration in ZnPc, which explains why the non-germinate recombination channel is not a main contributor to the triplet formation.

#### **CONCLUSION**

In summary, we have studied the ultrafast CT dynamics at the  $ZnPc\text{-}MoS_2$  interface. We demonstrate that effective electron transfer, with transfer time  $\sim 80$  fs, can occur at the interface to produce interfacial CT excitons. Because of the large singlet-triplet splitting of ZnPc, an electron in the TMD layer can transfer back to the organic layer to form a triplet exciton after the electron spin is flipped in  $MoS_2$ . The formation of triplet excitons can reduce the efficiency of carrier generation from the heterostructure. Therefore, the energy alignment at the organic-TMD interface must be probably tailored in order to avoid this process. On the other hand, the spin selective triplet formation process can be potentially used to manipulate electron spin in organic-TMD hybrid structures.

#### **METHODS**

# **Sample Preparation**

A single crystal  $MoS_2$  with the (0001) plane parallel to the surface was obtained from SPI Supplies. To provide mechanical support, the  $MoS_2$  crystal was mounted on a Si substrate using vacuum-compatible silver paint. Right before the sample was loaded into the vacuum chamber, the  $MoS_2$  surface was cleaved to expose a fresh surface. The sample was annealed at 350 °C for about 12 hours in an ultrahigh vacuum (UHV) chamber with a base pressure of  $1\times10^{-10}$  Torr. LEED and UPS were used to verify the surface cleanliness *via* the observation of a sharp diffraction pattern and sharp photoemission features. The sample was then transferred *in-situ* to another UHV chamber with a base pressure of  $8\times10^{-10}$  Torr where the ZnPc deposition was done. For

thicknesses less than 4 nm, the ZnPc molecules were deposited at a rate of 0.3 Å/min and a sample temperature of 90 °C to ensure a well-ordered film was formed (similar to the procedure reported in Ref. [35]). For thicknesses beyond 4 nm, the growth rate was increased to 0.7 Å/min and the sample was kept at room temperature. The same procedure is used to prepare the WSe<sub>2</sub> single crystal and the ZnPc films on WSe<sub>2</sub>.

## **UPS** spectroscopy

The UPS measurement was done with a standard UV lamp. The He-I emission line (21.2 eV) was used. During the UPS experiment, electrons were emitted continuously from the sample. For samples with a low conductivity, sample charging would occur which shifted the whole spectrum to lower electron kinetic energies. To avoid sample charging, a defocused, continuous-wave (CW) laser (533 nm) was used to irradiate the sample. The CW laser produced charge carriers in the MoS<sub>2</sub> crystal and increased its conductivity. The power of the laser was selected such that all the spectral shift due to the sample charging was removed (see supporting information).

## **TR-TPPE** spectroscopy

The TR-TPPE technique was used to study the CT dynamics. A pump energy of 1.77 eV and a probe energy of 4.68 eV were used. The pump pulses were obtained from the direct output of a non-collinear optical parametric amplifier (NOPA) - Light Conversion Orpheus-N-2H. The probe pulses was obtained from the second harmonic of the output of a second NOPA (Light Conversion Orpheus-N-3H). Both NOPAs were pumped by a Yb:KGW regenerative amplifier running at 125 kHz (Pharos, Light Conversion). The temporal cross correlation between the two pulses was 65 fs. The full-width half-maximum (fwhm) beam diameter at the sample was 0.8 mm. In the pump-fluence dependence experiment, the energy of the pump pulses was attenuated by neutral density filters. A hemispherical electron analyzer (Phoibos 100, SPECS) was used to measure the kinetic energy and the population of the ionized electrons. The TR-TPPE experiment were conducted at room temperature. In all the presented TPPE spectra, the one-photon photoemission background signal measured at negative delay times was subtracted. Hence, the signal in these spectra was contributed by two-photon photoemission.

## Photoluminescence spectroscopy

The photoluminescence spectra were taken using a 1.95 eV HeNe laser. The spectra were collected by a spectrometer after removing the HeNe wavelength using a notch filter. The experiment was conducted at room temperature. In each of the PL spectra presented a separate background scan was taken under the same conditions on the respective bare substrates. These background spectra were then subtracted from the initial measurements.

#### ASSOCIATED CONTENT

The Supporting information is available free of charges on the ACS Publications website Additional UPS, TR-TPPE spectra, data from control experiments

## **AUTHOR INFORMATION**

Corresponding Author
\* wlchan@ku.edu
Notes

The authors declare no competing financial interest.

#### **ACKNOWLEDGEMENT**

This work is primary supported by US National Science Foundation, grant DMR-1351716. This investigation was also supported by the University of Kansas New Faculty General Research Fund allocation #2302027. H. Z. acknowledges the support from US National Science Foundation, grant DMR-1505852.

# **REFERENCES**

- 1. Novoselov, K. S.; Mishchenko, A.; Carvalho, A.; Neto, A. H. C., 2D Materials and van der Waals Heterostructures. *Science* **2016**, *353*, 461.
- 2. Das, S.; Robinson, J. A.; Dubey, M.; Terrones, H.; Terrones, M., Beyond Graphene: Progress in Novel Two-Dimensional Materials and van der Waals Solids. *Annu Rev Mater Res* **2015**, *45*, 1-27.
- 3. Zhang, W. J.; Wang, Q. X.; Chen, Y.; Wang, Z.; Wee, A. T. S., Van Der Waals Stacked 2d Layered Materials for Optoelectronics. *2D Mater.* **2016**, *3*, 022001.
- 4. Wong, J.; Jariwala, D.; Tagliabue, G.; Tat, K.; Davoyan, A. R.; Sherrott, M. C.; Atwater, H. A., High Photovoltaic Quantum Efficiency in Ultrathin van der Waals Heterostructures. *ACS Nano* **2017**, *11*, 7230-7240.
- 5. Jariwala, D.; Marks, T. J.; Hersam, M. C., Mixed-Dimensional van der Waals Heterostructures. *Nat. Mater.* **2017**, *16*, 170-181.
- 6. Jariwala, D.; Dayoyan, A. R.; Tagliabue, G.; Sherrott, M. C.; Wong, J.; Atwater, H. A., Near-Unity Absorption in van der Waals Semiconductors for Ultrathin Optoelectronics. *Nano Lett.* **2016**, *16*, 5482-5487.
- 7. Lee, C. H.; Schiros, T.; Santos, E. J. G.; Kim, B.; Yager, K. G.; Kang, S. J.; Lee, S.; Yu, J.; Watanabe, K.; Taniguchi, T.; Hone, J.; Kaxiras, E.; Nuckolls, C.; Kim, P., Epitaxial Growth of Molecular Crystals on van der Waals Substrates for High-Performance Organic Electronics. *Adv. Mater.* **2014**, *26*, 2812-2817.
- 8. Jo, S. B.; Kim, H. H.; Lee, H.; Kang, B.; Lee, S.; Sim, M.; Kim, M.; Lee, W. H.; Cho, K., Boosting Photon Harvesting in Organic Solar Cells with Highly Oriented Molecular Crystals *via* Graphene-Organic Heterointerface. *ACS Nano* **2015**, *9*, 8206-8219.
- 9. Smith, M. B.; Michl, J., Singlet Fission. *Chem. Rev.* **2010**, *110*, 6891-6936.
- 10. McDonough, T. J.; Zhang, L. S.; Roy, S. S.; Kearns, N. M.; Arnold, M. S.; Zanni, M. T.; Andrew, T. L., Triplet Exciton Dissociation and Electron Extraction in Graphene-Templated Pentacene Observed with Ultrafast Spectroscopy. *PCCP* **2017**, *19*, 4809-4820.

- 11. Sun, D. L.; Ehrenfreund, E.; Vardeny, Z. V., The First Decade of Organic Spintronics Research. *Chem. Commun.* **2014**, *50*, 1781-1793.
- 12. Naber, W. J. M.; Faez, S.; van der Wiel, W. G., Organic Spintronics. *J Phys. D Appl. Phys.* **2007**, *40*, R205-R228.
- 13. Boehme, C.; Lupton, J. M., Challenges for Organic Spintronics. *Nat. Nanotechnol.* **2013**, *8*, 612-615.
- 14. Xu, X. D.; Yao, W.; Xiao, D.; Heinz, T. F., Spin and Pseudospins in Layered Transition Metal Dichalcogenides. *Nat. Phys.* **2014**, *10*, 343-350.
- 15. Xiao, D.; Liu, G. B.; Feng, W. X.; Xu, X. D.; Yao, W., Coupled Spin and Valley Physics in Monolayers of MoS<sub>2</sub> and Other Group-VI Dichalcogenides. *Phys. Rev. Lett.* **2012**, *108*, 196802.
- 16. Mak, K. F.; He, K. L.; Shan, J.; Heinz, T. F., Control of Valley Polarization in Monolayer Mos2 by Optical Helicity. *Nat. Nanotechnol.* **2012**, *7*, 494-498.
- 17. Hong, X. P.; Kim, J.; Shi, S. F.; Zhang, Y.; Jin, C. H.; Sun, Y. H.; Tongay, S.; Wu, J. Q.; Zhang, Y. F.; Wang, F., Ultrafast Charge Transfer in Atomically Thin MoS<sub>2</sub>/WS<sub>2</sub> Heterostructures. *Nat. Nanotechnol.* **2014**, *9*, 682-686.
- 18. Ceballos, F.; Bellus, M. Z.; Chiu, H. Y.; Zhao, H., Ultrafast Charge Separation and Indirect Exciton Formation in a MoS<sub>2</sub>-MoSe<sub>2</sub> van der Waals Heterostructure. *ACS Nano* **2014**, *8*, 12717-12724.
- 19. Zhu, H.; Wang, J.; Gong, Z.; Kim, Y. D.; Hone, J.; Zhu, X. Y., Interfacial Charge Transfer Circumventing Momentum Mismatch at Two-Dimensional van der Waals Heterojunctions. *Nano Lett.* **2017**, *17*, 3591-3598.
- 20. Nguyen, E. P.; Carey, B. J.; Harrison, C. J.; Atkin, P.; Berean, K. J.; Della Gaspera, E.; Ou, J. Z.; Kaner, R. B.; Kalantar-Zadeh, K.; Daeneke, T., Excitation Dependent Bidirectional Electron Transfer in Phthalocyanine-Functionalised MoS<sub>2</sub> Nanosheets. *Nanoscale* **2016**, *8*, 16276-16283.
- 21. Choi, J.; Zhang, H. Y.; Choi, J. H., Modulating Optoelectronic Properties of Two Dimensional Transition Metal Dichalcogenide Semiconductors by Photoinduced Charge Transfer. *ACS Nano* **2016**, *10*, 1671-1680.
- 22. Jariwala, D.; Howell, S. L.; Chen, K. S.; Kang, J. M.; Sangwan, V. K.; Filippone, S. A.; Turrisi, R.; Marks, T. J.; Lauhon, L. J.; Hersam, M. C., Hybrid, Gate-Tunable, van der Waals p-n Heterojunctions from Pentacene and MoS<sub>2</sub>. *Nano Lett.* **2016**, *16*, 497-503.
- 23. Velez, S.; Ciudad, D.; Island, J.; Buscema, M.; Txoperena, O.; Parui, S.; Steele, G. A.; Casanova, F.; van der Zant, H. S. J.; Castellanos-Gomez, A.; Hueso, L. E., Gate-Tunable Diode and Photovoltaic Effect in an Organic-2D Layered Material p-n Junction. *Nanoscale* **2015**, *7*, 15442-15449.
- 24. Liu, X.; Gu, J.; Ding, K.; Fan, D. J.; Hu, X. E.; Tseng, Y. W.; Lee, Y. H.; Menon, V.; Forrest, S. R., Photoresponse of an Organic Semiconductor/Two-Dimensional Transition Metal Dichalcogenide Heterojunction. *Nano Lett.* **2017**, *17*, 3176-3181.
- 25. Chen, R. F.; Lin, C.; Yu, H.; Tang, Y. T.; Song, C.; Yuwen, L. H.; Li, H.; Xie, X. J.; Wang, L. H.; Huang, W., Templating C-60 on MoS<sub>2</sub> Nanosheets for 2D Hybrid van der Waals p-n Nanoheterojunctions. *Chem. Mater.* **2016**, *28*, 4300-4306.
- 26. Homan, S. B.; Sangwan, V. K.; Balla, I.; Bergeron, H.; Weiss, E. A.; Hersam, M. C., Ultrafast Exciton Dissociation and Long-Lived Charge Separation in a Photovoltaic Pentacene-MoS<sub>2</sub> van der Waals Heterojunction. *Nano Lett.* **2017**, *17*, 164-169.
- 27. Petoukhoff, C. E.; Krishna, M. B. M.; Voiry, D.; Bozkurt, I.; Deckoff-Jones, S.; Chhowalla, M.; O'Carroll, D. M.; Dani, K. M., Ultrafast Charge Transfer and Enhanced

- Absorption in MoS<sub>2</sub>-Organic van der Waals Heterojunctions Using Plasmonic Metasurfaces. *ACS Nano* **2016**, *10*, 9899-9908.
- 28. Sharma, D.; Huijser, A.; Savolainen, J.; Steen, G.; Herek, J. L., Active and Passive Control of Zinc Phthalocyanine Photodynamics. *Faraday Discuss.* **2013**, *163*, 433-445.
- 29. Sun, Y. R.; Giebink, N. C.; Kanno, H.; Ma, B. W.; Thompson, M. E.; Forrest, S. R., Management of Singlet and Triplet Excitons for Efficient White Organic Light-Emitting Devices. *Nature* **2006**, *440*, 908-912.
- 30. Rao, A.; Chow, P. C. Y.; Gelinas, S.; Schlenker, C. W.; Li, C. Z.; Yip, H. L.; Jen, A. K. Y.; Ginger, D. S.; Friend, R. H., The Role of Spin in the Kinetic Control of Recombination in Organic Photovoltaics. *Nature* **2013**, *500*, 435-439.
- 31. Mak, K. F.; Lee, C.; Hone, J.; Shan, J.; Heinz, T. F., Atomically Thin MoS<sub>2</sub>: A New Direct-Gap Semiconductor. *Phys. Rev. Lett.* **2010**, *105*, 136805.
- 32. Ramasubramaniam, A., Large Excitonic Effects in Monolayers of Molybdenum and Tungsten Dichalcogenides. *Phys. Rev. B* **2012**, *86*.
- 33. Ugeda, M. M.; Bradley, A. J.; Shi, S. F.; da Jornada, F. H.; Zhang, Y.; Qiu, D. Y.; Ruan, W.; Mo, S. K.; Hussain, Z.; Shen, Z. X.; Wang, F.; Louie, S. G.; Crommie, M. F., Giant Bandgap Renormalization and Excitonic Effects in a Monolayer Transition Metal Dichalcogenide Semiconductor. *Nat. Mater.* **2014**, *13*, 1091-1095.
- 34. Padilha, J. E.; Peelaers, H.; Janotti, A.; Van de Walle, C. G., Nature and Evolution of the Band-Edge States in MoS<sub>2</sub>: From Monolayer to Bulk. *Phys. Rev. B* **2014**, *90*, 205420.
- 35. England, C. D.; Collins, G. E.; Schuerlein, T. J.; Armstrong, N. R., Epitaxial Thin-Films of Large Organic-Molecules Characterization of Phthalocyanine and Coronene Overlayers on the Layered Semiconductors MoS<sub>2</sub> and SnS<sub>2</sub>. *Langmuir* **1994**, *10*, 2748-2756.
- 36. Chen, W.; Huang, H.; Chen, S.; Huang, Y. L.; Gao, X. Y.; Wee, A. T. S., Molecular Orientation-Dependent Ionization Potential of Organic Thin Films. *Chem. Mater.* **2008**, *20*, 7017-7021.
- 37. Wang, T.; Kafle, T. R.; Kattel, B.; Liu, Q. F.; Wu, J.; Chan, W. L., Growing Ultra-Flat Organic Films on Graphene with a Face-on Stacking *via* Moderate Molecule-Substrate Interaction. *Sci. Rep.* **2016**, *6*, 28895.
- 38. Han, S. W.; Cha, G. B.; Frantzeskakis, E.; Razado-Colambo, I.; Avila, J.; Park, Y. S.; Kim, D.; Hwang, J.; Kang, J. S.; Ryu, S.; Yun, W. S.; Hong, S. C.; Asensio, M. C., Band-Gap Expansion in the Surface-Localized Electronic Structure of MoS<sub>2</sub>(0002). *Phys. Rev. B* **2012**, *86*, 115105.
- 39. Cheiwchanchamnangij, T.; Lambrecht, W. R. L., Quasiparticle Band Structure Calculation of Monolayer, Bilayer, and Bulk MoS<sub>2</sub>. *Phys. Rev. B* **2012**, *85*, 205302.
- 40. Davidson, A. T., The Effect of the Metal Atom on the Absorption-Spectra of Phthalocyanine Films. *J. Chem. Phys.* **1982**, *77*, 168-172.
- 41. Zhu, X. Y., Electronic Structure and Electron Dynamics at Molecule-Metal Interfaces: Implications for Molecule-Based Electronics. *Surf. Sci. Rep.* **2004**, *56*, 1-83.
- 42. Wang, T.; Liu, Q. F.; Caraiani, C.; Zhang, Y. P.; Wu, J.; Chan, W. L., Effect of Interlayer Coupling on Ultrafast Charge Transfer from Semiconducting Molecules to Mono- and Bilayer Graphene. *Phys. Rev. Appl.* **2015**, *4*, 014016.
- 43. Jnawali, G.; Rao, Y.; Beck, J. H.; Petrone, N.; Kymissis, I.; Hone, J.; Heinz, T. F., Observation of Ground- and Excited-State Charge Transfer at the C-60/Graphene Interface. *ACS Nano* **2015**, *9*, 7175-7185.

- 44. Zheng, Y. J.; Huang, Y. L.; Chenp, Y. F.; Zhao, W. J.; Eda, G.; Spataru, C. D.; Zhang, W. J.; Chang, Y. H.; Li, L. J.; Chi, D. Z.; Quek, S. Y.; Wee, A. T. S., Heterointerface Screening Effects between Organic Monolayers and Monolayer Transition Metal Dichalcogenides. *ACS Nano* **2016**, *10*, 2476-2484.
- 45. Yoshino, K.; Hikida, M.; Tatsuno, K.; Kaneto, K.; Inuishi, Y., Emission-Spectra of Phthalocyanine Crystals. *J. Phys. Soc. Jpn.* **1973**, *34*, 441-445.
- 46. Wang, L.; Wu, M. W., Electron Spin Relaxation Due to D'yakonov-Perel' and Elliot-Yafet Mechanisms in Monolayer MoS<sub>2</sub>: Role of Intravalley and Intervalley Processes. *Phys. Rev. B* **2014**, *89*, 115302.
- 47. Chen, X.; Yan, T. F.; Zhu, B. R.; Yang, S. Y.; Cui, X. D., Optical Control of Spin Polarization in Monolayer Transition Metal Dichalcogenides. *ACS Nano* **2017**, *11*, 1581-1587.
- 48. Yang, L. Y.; Sinitsyn, N. A.; Chen, W. B.; Yuan, J. T.; Zhang, J.; Lou, J.; Crooker, S. A., Long-Lived Nanosecond Spin Relaxation and Spin Coherence of Electrons in Monolayer MoS<sub>2</sub> and WS<sub>2</sub>. *Nat. Phys.* **2015**, *11*, 830-834.
- 49. Beal, A. R.; Hughes, H. P., Kramers-Kronig Analysis of the Reflectivity Spectra of 2H-MoS<sub>2</sub>, 2H-MoSe<sub>2</sub> and 2H-MoTe<sub>2</sub>. *J Phys. C Solid State* **1979**, *12*, 881-890.
- 50. Hufner, S., *Photoemission Spectroscopy: Principles and Applications*; Springer-Verlag: Berlin, 2003.
- 51. Johannsen, J. C.; Ulstrup, S.; Cilento, F.; Crepaldi, A.; Zacchigna, M.; Cacho, C.; Turcu, I. C. E.; Springate, E.; Fromm, F.; Raidel, C.; Seyller, T.; Parmigiani, F.; Grioni, M.; Hofmann, P., Direct View of Hot Carrier Dynamics in Graphene. *Phys. Rev. Lett.* **2013**, *111*, 027403.
- 52. Wallauer, R.; Reimann, J.; Armbrust, N.; Gudde, J.; Hofer, U., Intervalley Scattering in MoS<sub>2</sub> Imaged by Two-Photon Photoemission with a High-Harmonic Probe. *Appl. Phys. Lett.* **2016**, *109*, 162102.
- 53. Wang, T.; Chan, W. L., Dynamical Localization Limiting the Coherent Transport Range of Excitons in Organic Crystals. *J. Phys. Chem. Lett.* **2014**, *5*, 1812-1818.
- 54. Wang, T.; Kafle, T. R.; Kattel, B.; Chan, W.-L., A Multidimensional View of Charge Transfer Excitons at Organic Donor–Acceptor Interfaces. *J. Am. Chem. Soc.* **2017**, *139*, 4098-4106.
- 55. Shi, H.; Yan, R.; Bertolazzi, S.; Brivio, J.; Gao, B.; Kis, A.; Jena, D.; Xing, H. G.; Huang, L., Exciton Dynamics in Suspended Monolayer and Few-Layer MoS<sub>2</sub> 2D Crystals. *ACS Nano* **2013**, *7*, 1072-1080.
- 56. Kumar, N.; He, J.; He, D.; Wang, Y.; Zhao, H., Charge Carrier Dynamics in Bulk MoS<sub>2</sub> Crystal Studied by Transient Absorption Microscopy. *J. Appl. Phys.* **2013**, *113*, 133702.
- 57. Riley, J. M.; Mazzola, F.; Dendzik, M.; Michiardi, M.; Takayama, T.; Bawden, L.; Granerod, C.; Leandersson, M.; Balasubramanian, T.; Hoesch, M.; Kim, T. K.; Takagi, H.; Meevasana, W.; Hofmann, P.; Bahramy, M. S.; Wells, J. W.; King, P. D. C., Direct Observation of Spin-Polarized Bulk Bands in an Inversion-Symmetric Semiconductor. *Nat. Phys.* **2014**, *10*, 835-839.
- 58. Traving, M.; Boehme, M.; Kipp, L.; Skibowski, M.; Starrost, F.; Krasovskii, E. E.; Perlov, A.; Schattke, W., Electronic Structure of Wse2: A Combined Photoemission and Inverse Photoemission Study. *Phys. Rev. B* **1997**, *55*, 10392-10399.
- 59. Morozov, Y. V.; Kuno, M., Optical Constants and Dynamic Conductivities of Single Layer MoS<sub>2</sub>, MoSe<sub>2</sub>, and WSe<sub>2</sub>. *Appl. Phys. Lett.* **2015**, *107*, 083103.

## **Figure Captions:**

Figure 1: (a) The LEED pattern for the single crystal  $MoS_2$  prior to ZnPc deposition. The energy of the electron beam is shown on the figure. (b) The LEED pattern for 1 nm-ZnPc on  $MoS_2$ . (c) UPS spectra for the bare  $MoS_2$ , and ZnPc on  $MoS_2$  with different ZnPc thicknesses. The solid triangles and the red vertical line represent the  $MoS_2$ 's Mo-4d band and VBM respectively. Blue vertical lines indicate the position of the ZnPc's HOMO. (d) The energy level diagram at the  $MoS_2$ -ZnPc interface. Electronic processes including (i) optical excitation; (ii) charge transfer (CT); and (iii) back electron transfer (BET) are indicated on the figure. (e) The PL spectra for 2 nm ZnPc films grown on  $SiO_2$  (300 nm)/Si and  $MoS_2$  substrates.

Figure 2: (a-b) The TR-TPPE spectrum of the 0.5 nm-ZnPc on MoS<sub>2</sub> sample shown in two different time ranges. (c) The TR-TPPE spectrum of 1 nm-ZnPc on MoS<sub>2</sub>. In both the 0.5 nm and 1 nm spectra, the decay of the S<sub>1</sub> state on the 100 fs timescale and the rise of the T<sub>1</sub> state on the ps timescale can be observed. (d) The TR-TPPE spectrum of 10 nm-ZnPc on MoS<sub>2</sub>. The S<sub>1</sub> excitons near the sample surface are not affected by the CT occurring at the ZnPc-MoS<sub>2</sub> interface on this short timescale, which results in the long S<sub>1</sub> lifetime.

Figure 3: (a) TPPE spectra at selected delay times for the 0.5 nm-ZnPc on MoS<sub>2</sub> sample. (b) The temporal evolution of the intensity of the S<sub>1</sub> state for different ZnPc thicknesses. The fast intensity decay in the thinner samples (0.5 nm and 1 nm) is attributed to CT to MoS<sub>2</sub>. An exponential fit (dashed line) shows a decay time of 80 fs. (c) The temporal evolution of the intensity of the T<sub>1</sub> state for different ZnPc thicknesses. For the 1 nm sample, the intensity rise is fit with a biexponential function (dashed line). Time constants of 2.7 and 81 ps are found.

Figure 4: (a) The band alignment at the ZnPc-bulk WSe<sub>2</sub> interface measured by our UPS experiment. (b) The TR-TPPE spectrum for the 1 nm ZnPc-WSe<sub>2</sub> sample. The S<sub>1</sub> state of ZnPc at  $\sim 1.7$  eV can be identified. (c) The temporal evolution of the intensity of the S<sub>1</sub> state. The dashed line is an exponential fit to the intensity decay. A decay time of 230 fs is obtained.

Figure 5: The intensity evolution of the T<sub>1</sub> state for the 1 nm-ZnPc sample. Three different pump laser fluences are used. The curves shown in the main panel are normalized. The kinetics is essentially independent of the pump fluences. The inset shows the actual TPPE intensity at 200 ps as a function of the laser fluence. A linear dependence is found.

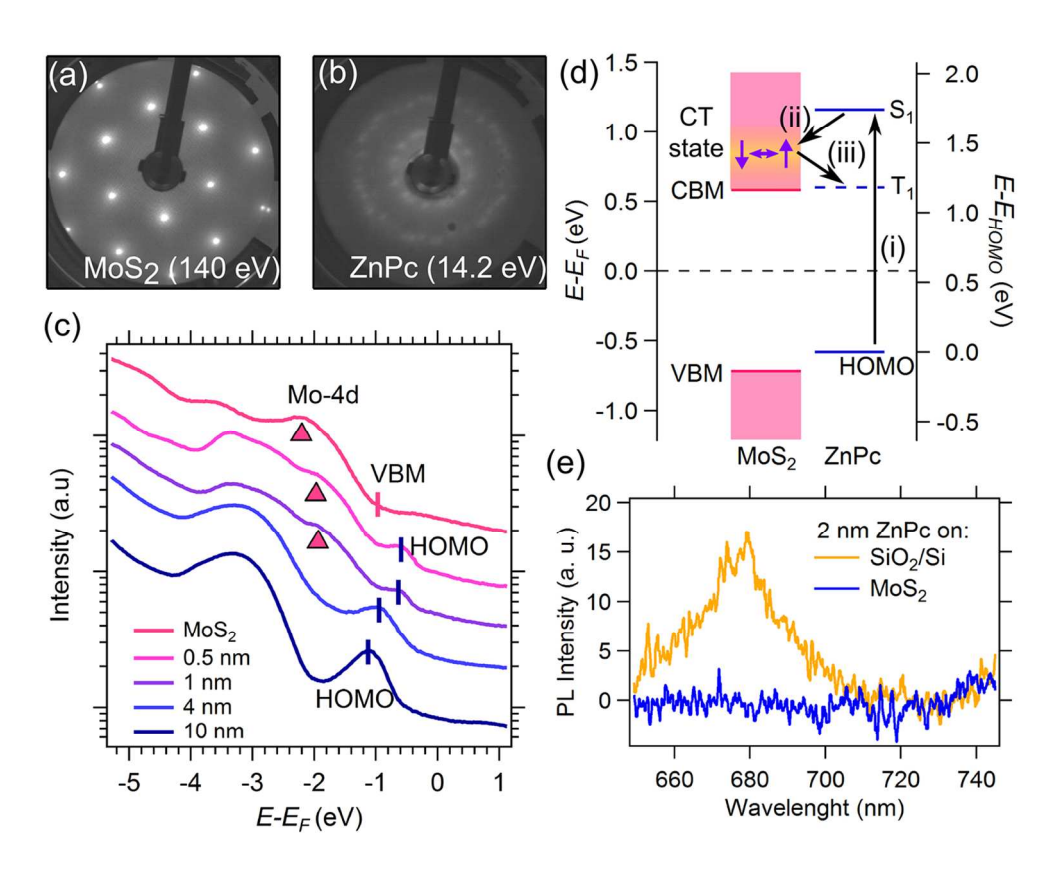


Figure 1: (a) The LEED pattern for the single crystal  $MoS_2$  prior to ZnPc deposition. The energy of the electron beam is shown on the figure. (b) The LEED pattern for 1 nm-ZnPc on  $MoS_2$ . (c) UPS spectra for the bare  $MoS_2$ , and ZnPc on  $MoS_2$  with different ZnPc thicknesses. The solid triangles and the red vertical line represent the  $MoS_2$ 's Mo-4d band and VBM respectively. Blue vertical lines indicate the position of the ZnPc's HOMO. (d) The energy level diagram at the  $MoS_2$ -ZnPc interface. Electronic processes including (i) optical excitation; (ii) charge transfer (CT); and (iii) back electron transfer (BET) are indicated on the figure. (e) The PL spectra for 2 nm ZnPc films grown on  $SiO_2$  (300 nm)/Si and  $MoS_2$  substrates.

127x102mm (300 x 300 DPI)

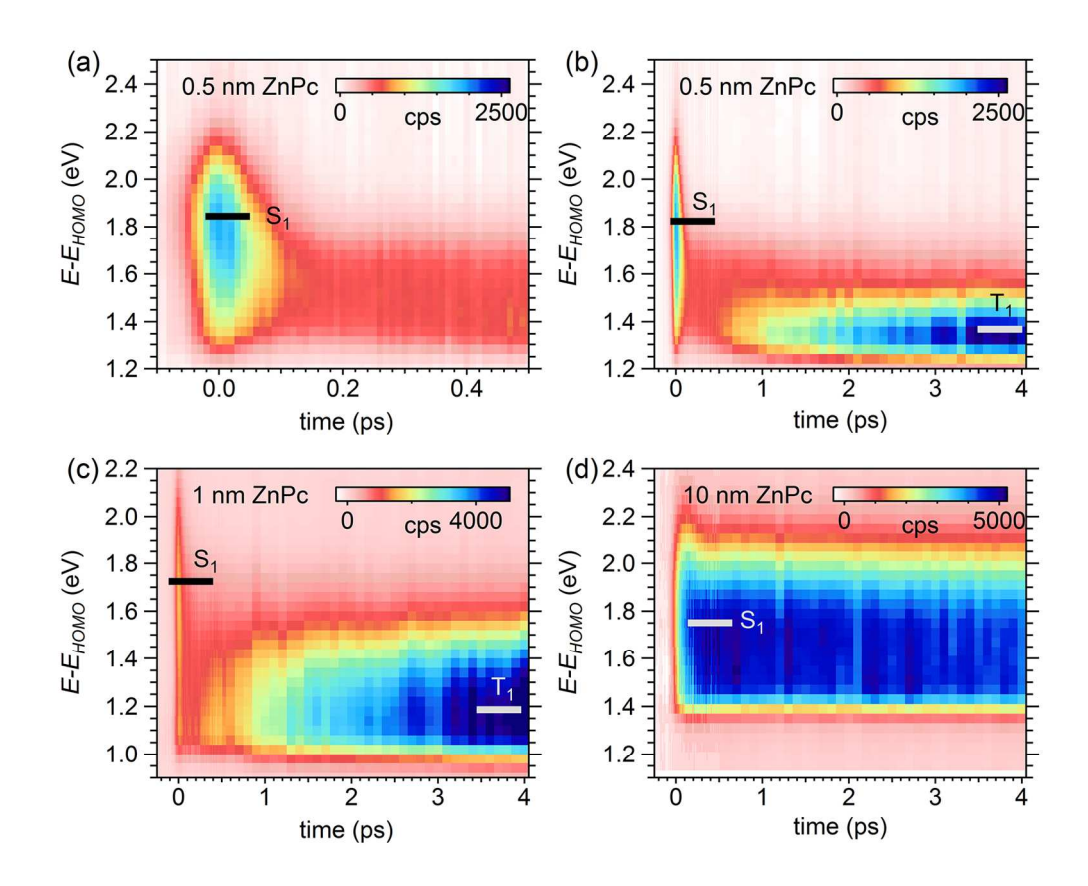


Figure 2:(a-b) The TR-TPPE spectrum of the 0.5 nm-ZnPc on  $MoS_2$  sample shown in two different time ranges. (c) The TR-TPPE spectrum of 1 nm-ZnPc on  $MoS_2$ . In both the 0.5 nm and 1 nm spectra, the decay of the  $S_1$  state on the 100 fs timescale and the rise of the  $T_1$  state on the ps timescale can be observed. (d) The TR-TPPE spectrum of  $T_1$  nm-ZnPc on  $T_2$  near the sample surface are not affected by the CT occurring at the  $T_1$  state on this short timescale, which results in the long  $T_2$  lifetime.

152x125mm (300 x 300 DPI)

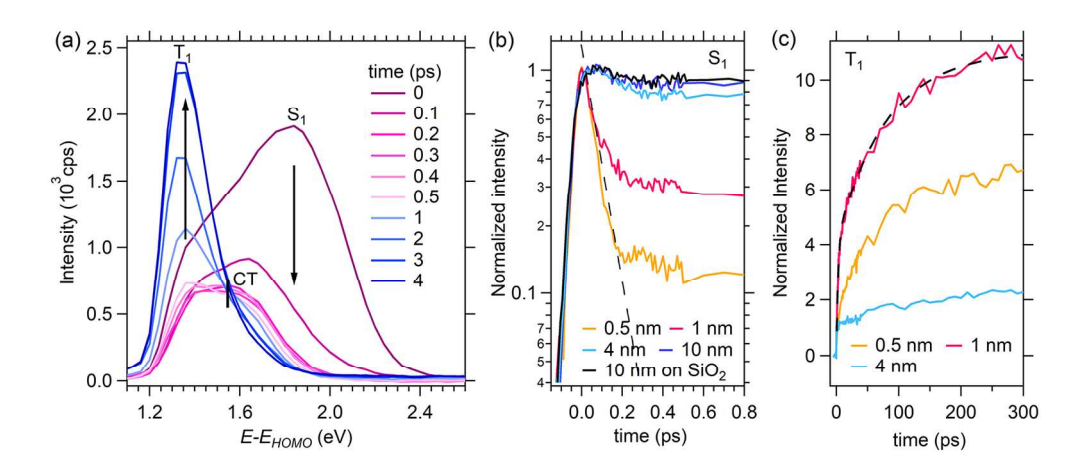


Figure 3: (a) TPPE spectra at selected delay times for the 0.5 nm-ZnPc on  $MoS_2$  sample. (b) The temporal evolution of the intensity of the  $S_1$  state for different ZnPc thicknesses. The fast intensity decay in the thinner samples (0.5 nm and 1 nm) is attributed to CT to  $MoS_2$ . An exponential fit (dashed line) shows a decay time of 80 fs. (c) The temporal evolution of the intensity of the  $T_1$  state for different ZnPc thicknesses. For the 1 nm sample, the intensity rise is fit with a bi-exponential function (dashed line). Time constants of 2.7 and 81 ps are found.

152x65mm (300 x 300 DPI)

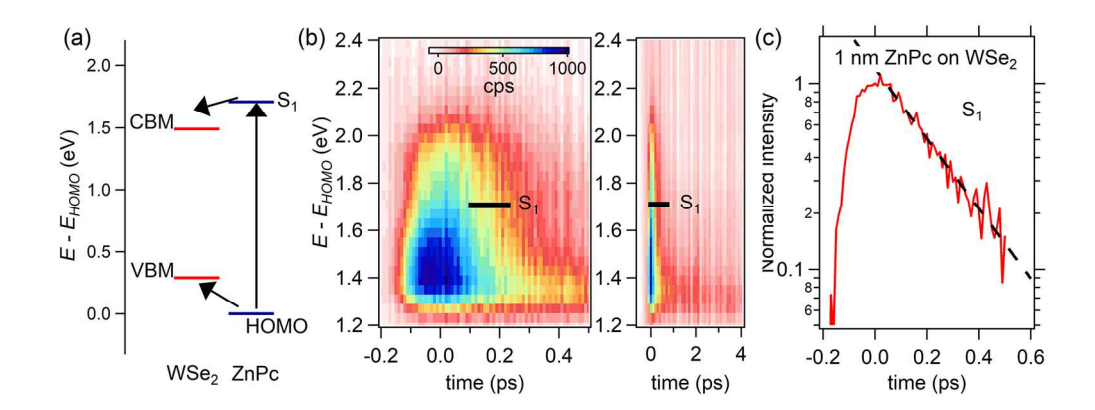


Figure 4: (a) The band alignment at the ZnPc-bulk WSe $_2$  interface measured by our UPS experiment. (b) The TR-TPPE spectrum for the 1 nm ZnPc-WSe $_2$  sample. The S $_1$  state of ZnPc at  $\sim 1.7$  eV can be identified. (c) The temporal evolution of the intensity of the S $_1$  state. The dashed line is an exponential fit to the intensity decay. A decay time of 230 fs is obtained.

157x59mm (300 x 300 DPI)

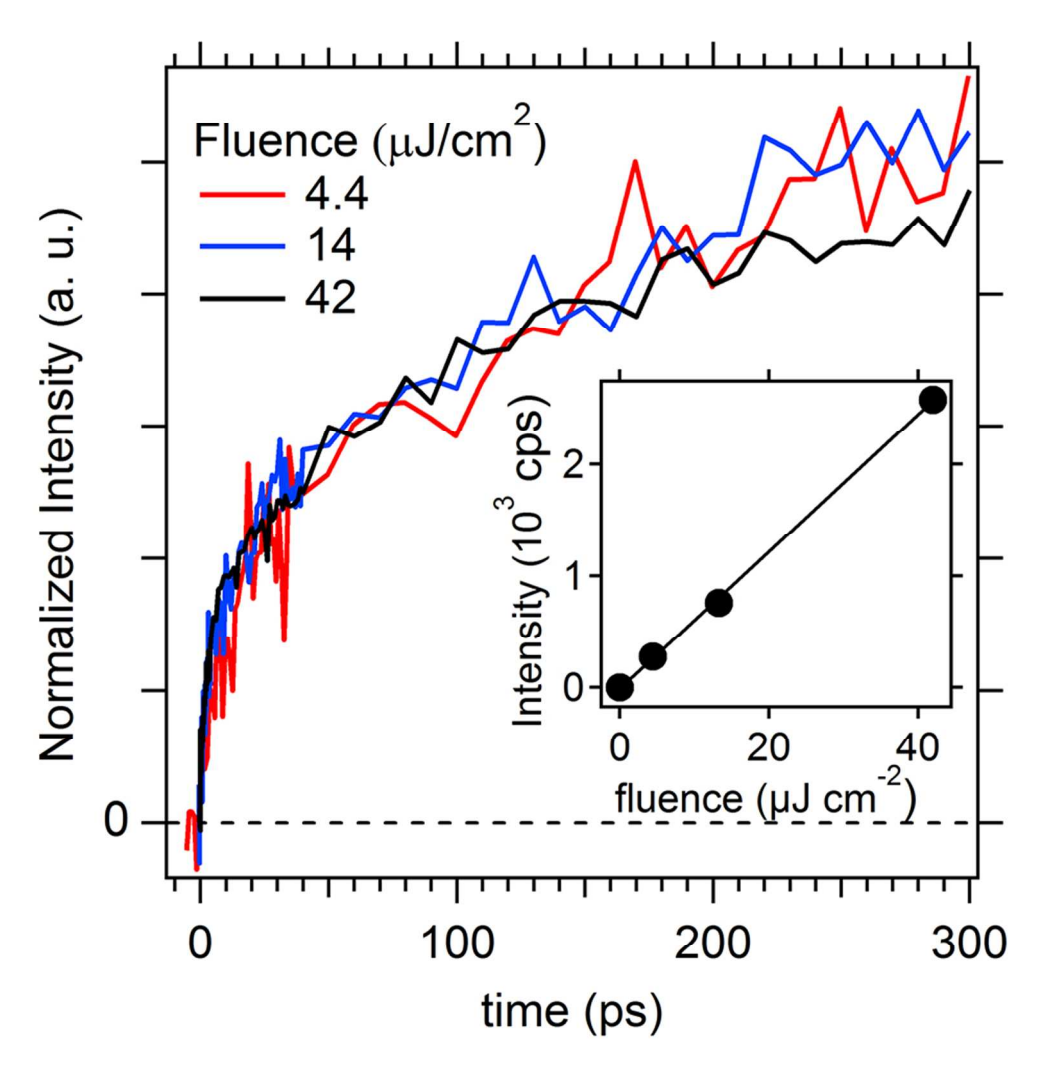
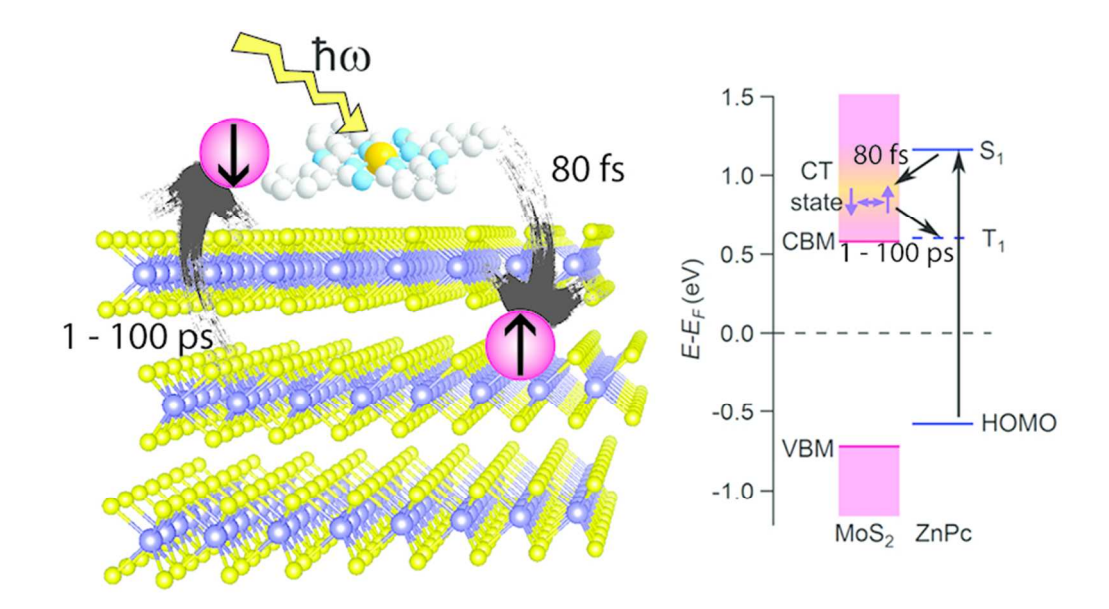


Figure 5: The intensity evolution of the  $T_1$  state for the 1 nm-ZnPc sample. Three different pump laser fluences are used. The curves shown in the main panel are normalized. The kinetics is essentially independent of the pump fluences. The inset shows the actual TPPE intensity at 200 ps as a function of the laser fluence. A linear dependence is found.

81x83mm (300 x 300 DPI)



TOC figure 71x39mm (300 x 300 DPI)